Shadow-Effect Correction in Aerial Color Imagery

Hong-Gyoo Sohn and Kong-Hyun Yun

Abstract

Due to the existence of shadows, especially in urban environments, it is difficult to extract semantic information from aerial and high-resolution satellite images. In this paper, an efficient method of correcting shadow effects using multi-source data sets in aerial color images is proposed. The proposed method has three steps. First, it accurately detects the shadowed regions using the image geometry and the solar position of the image acquisition data. Then, the detected shadowed regions are segmented according to land surface type. Finally, the shadow effects of the segmented regions are corrected by directly comparing the same non-shadow features with the segmented shadows. In the application part of this paper, the proposed techniques were applied in the extraction of an asphalt road from an image.

Introduction

In remotely sensed imagery, shadows can sometimes be used to extract geospatial information. However, shadows sometimes have a negative effect on the extraction of geometric and semantic information on the earth's surface especially in urban environments, because shadows cast by high-rise ground objects make it difficult to implement photogrammetric applications such as feature extraction, automatic triangulation, and orthophoto generation.

Intensive research has been implemented to correct shadow effects in remotely sensed images (Pouch and Compagna, 1990; Colby, 1991; Itten and Meyer, 1993; Richter, 1998; Kawata *et al.*, 1998; Simpson and Stitt, 1998; Rau *et al.*, 2002; Dare, 2005). Most research on shadow detection and removal has been done, however, on mountainous terrain using satellite images (Hall-Konyves, 1987; Civco, 1989; Lui and Moore, 1993; Wang *et al.*, 1999; Giles, 2001). Because mountainous areas are composed mainly of forests, the correction of shadow effects is relatively easy in this regard compared to that on images with complex built-up urban environments. Simpson and Stitt (1998) removed cloud shadows from AVHRR data using geometric considerations to project the cloud features on the ground in the direction of a solar azimuth angle and the cloud height. Wang *et al.* (1999) proposed the automated algorithm to detect and remove cloud shadows from Landsat TM data based on changes in the reflectance and frequency components and replacement with the acquired non-shadow image at a different time. Giles (2001) also investigated the shadow detection algorithm from a Landsat TM image and described a quantitative spatial evaluation of the proposed method in comparison to manual interpretation.

On the treatment of shadows in urban areas, Rau *et al.* (2002) have observed that shadow effects could be corrected using the histogram matching method, which is applied to minimize the gray value differences between a shadowed area and its surroundings in the process of producing *true* orthoimages. The histogram matching method is also used to remove shadows in aerial photographs (Shu and Freeman, 1990). Moreover, Dare (2005) showed that shadows could be removed with the histogram adjustment method in built-up urban areas. Although, the results can be image-dependent.

In addition to the methods used in the abovementioned researches, novel methods such as spectral end-members and the matched filter concept are used to remove shadows (Boardman, 1993; Adler-Golden *et al.*, 2002).

This study attempts to correct shadow effects in aerial color imagery using multi-source data sets. To detect the shadowed regions, digital maps and lidar data were selected to generate Digital Elevation Model (DEM) and Digital Surface Model (DSM), respectively. To avoid confusion of acronyms such as DEM and DSM in this paper, DEM was defined as a model that represents a topographic surface, and DSM, as a model that delineates the canopy of the object surface.

The shadowed regions were accurately modeled using the geometric relationship between a three-dimensional model of the research area and the solar position of the image acquisition data. Also, to accurately correct the shadow effects, the shadowed regions were segmented using an existing digital map, which included the land surface cover types. Afterwards, based on the three proposed basic assumptions, the identified shadowed regions were given new calculated values. In the last part of this paper, to evaluate the proposed scheme, the potential application of asphalt road extraction using only a digital aerial image and lidar data is presented.

Data Preparation

The study site and the data sets were carefully selected for this research to test the proposed method. The used data sets consisted of a mosaic of aerial color imagery, lidar data, and digital maps with a scale of 1:1000. The study site was in some parts of Sungnam City (approximately 127.01°E, 37.36°N), Korea. The aerial color image was acquired on

Hong-Gyoo Sohn is with the School of Civil and Environmental Engineering, Yonsei University, 134 Shinchon-Dong Seodaemun-Gu, Seoul,120-749, Korea.

Kong-Hyun Yun is with the Construction Engineering Research Institute, Yonsei University, 134 Shinchon-Dong Seodaemun-Gu, Seoul,120-749, Korea (ykh1207@yonsei.ac.kr).

Photogrammetric Engineering & Remote Sensing
Vol. 74, No. 5, May 2008, pp. 611–618.

0099-1112/08/7405–0611/$3.00/0

Plate 1. Aerial color image of study area.

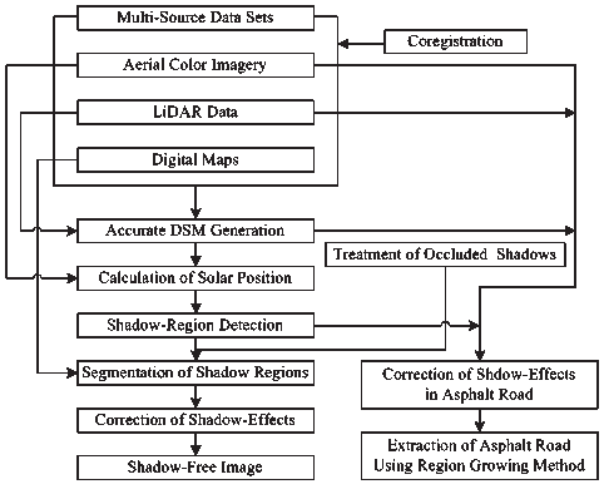

Figure 1. Schematic diagram of the proposed method.

the 10 December 2002, at approximately 1119 local time, which corresponded to early winter and cast long shadows on the ground surfaces. As shown in Plate 1, the image contains buildings, trees, roads, streets, grass, parking lots, and other urban features.

The aerial color photos were scanned at 50 μm, making the pixel resolution approximately 25 cm on the ground. The aerial image was orthorectified using digital maps and mosaic. The overall accuracy of the orthorectified image was approximately 0.75 m. The ground height was approximately 30 to 55 meters and the height of the buildings was about 45 to 150 meters from the mean sea level. The DEM was generated with the triangulated irregular network (TIN) method using spot heights and elevation contours from 1:1000-scale digital maps, and was converted into a grid format at a 25 cm grid interval.

The building height came from lidar, which is an active technique of acquiring 3D information describing the land surface. Optech, Inc. acquired the lidar data on the 04 April 2004 using the ALTM1020 system with a 5 KHZ laser repetition rate. The terrain was scanned at a $\pm 9^{\circ}$ off-nadir angle as the aircraft flew at approximately 800 m AGL. The lidar data were co-registered into images and a digital map using the polynomial method.

The Proposed Approach

Figure 1 shows a flowchart of the proposed scheme, which includes its main steps: data co-registration, detection of shadowed regions, segmentation of shadowed regions, correction of shadow effects, and potential application to asphalt road extraction. In the process of co-registration, aerial color images are rectified and mosaiced with digital maps. Also, to accurately detect the shadowed regions, lidar data should be shifted due to their horizontal error. In this paper, the peak points of the lidar data between the building boundaries and the ground were used for the registration. The difference between the coordinates of the peak points and the building boundaries of the image was calculated and utilized for the horizontal shift of all the lidar data.

In the generation of DEM, spot heights and elevation contours of digital maps are used through the TIN method. Next, the building layer is extracted from the digital map: in particular, the building polygon, out of the map's many urban-environment-related features. Generally, the building polygons of digital maps are represented as single polygons and cover the ground area. However, as illustrated in Plate 1, the upper part of the building was mostly not flat but undulating. For accurate modeling, a polygon representing the rising part of the building was added to the building layer. Therefore, the building heights that were acquired as mean values of the lidar data within each polygon were entered. Subsequently, the shadowed regions were delineated by geometric relationships that included the calculated solar positions and the urban surface models. In addition to this work, DSM, which represented the canopy of the ground object surface, was generated using only the lidar data from a simple interpolation technique.

In the next stage, the detected shadowed regions are segmented according to land surface type using the attribute date of the digital maps. Finally, the shadow effects were corrected for each of the segmented shadowed regions. Also, the test for the possibility of ground feature extraction is implemented.

Detection of Shadow Regions

Detection of shadowed regions serves to calculate shadow length using height data from lidar data, the sun elevation angle, and the azimuth of the sun.

Before detecting shadowed regions, the accurate height value of a building must be acquired for precise shadow effect correction. The building height could be acquired directly using lidar data. The lidar data within the building polygon had two homogeneous values. One value represented the height of the bulk of the building, while the other value represented the building height except its bulk. However, the building polygon was shown as one polygon in the digital map. To solve this problem, a polygon representing the bulk of the building was added. The boundary between the bulk and other part was delineated. In other words, one polygon was created by grouping peak points above 1.0 m in comparison with the average of the lidar data within the polygon. Figure 2 shows the results of DSM, which is composed of DEM and the building height.

To detect shadowed regions, in addition to building height, solar positions are required at the time of image acquisition. To calculate the solar positions (the sun elevation angle and the azimuth), the accurate time, date, latitude, and longitude of the study area are needed. The image was

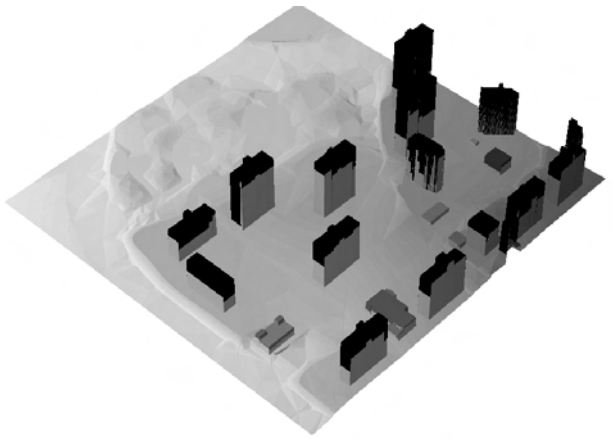

Figure 2. DSM generation using lidar data and digital maps

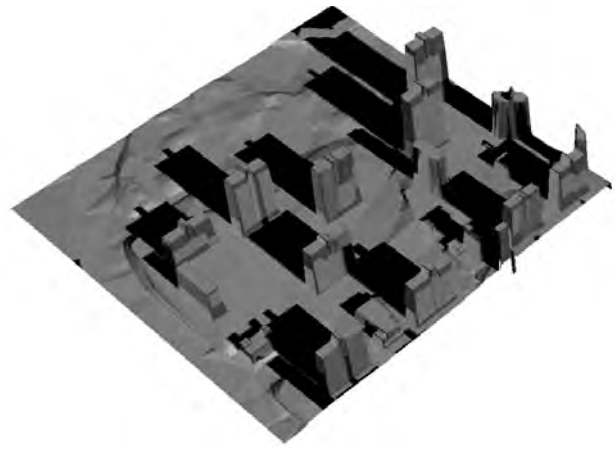

Figure 4. Result of shadow detection.

acquired on 10 November 2002 at 1119 local time. The longitude of the study area was 127° 06′ 58″N and the latitude was 37° 22′ 01″E. If the building height and the sun elevation angle could be acquired, the detection of shadows would be possible. Figure 3 represents the geometry between the building height, the elevation angle, and the length of the shadow in one dimension.

The solar elevation angle and the azimuth angel were calculated by the equations used by National Oceanic and Atmospheric Administration (NOAA) in calculating sunrise/sunset and solar position (Details can be accessed from NOAA website: **www.srrb.noaa.gov/highlights/sunrise/calcdetails.html**). Through equations, the solar elevation of 29.793° and the solar azimuth of 179.389° were calculated. Figure 4 shows the results of extraction of shadow regions using building height and the calculated solar elevation and azimuth.

Treatment of Occluded Shadow Regions

The test image used in this study was not recently initiated *true* orthophoto which is generated by removing object relief displacement. So, the relief displacement caused by buildings remains in the test image. Therefore, the shadow generated by shadow modeling is different from that of original image. For solving discrepancy it is necessary to extract the shadow regions partially occluded by buildings. As described in Figure 5, occluded regions can be obtained by performing 2D polygon boolean operations between modeled shadow polygon and building boundary polygon in aerial image. In other words, regions to be corrected for shadow effect actually can be extracted when modeled shadow region is separated from building boundary area ($\square ACC'D'B'B$). Extracting building boundary is possible by calculating the coordinates of vertices of building boundary using collinearity Equations 1 and 2. Using known photo orientation parameters (interior and exterior orientation parameters) and DSM, it is possible to determine the corresponding image coordinates (x, y) for object coordinates (X, Y, Z). As showed in Figure 5, the ground coordinates of points A, B, C, and D would be projected into the image plane points A′, B′, C′, and D′,

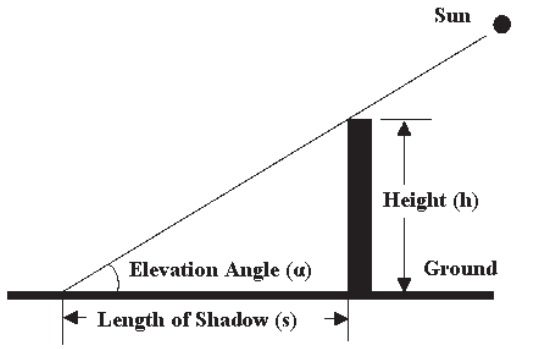

Figure 3. The geometry between height, elevation angle and length of shadow at fixed azimuth angle.

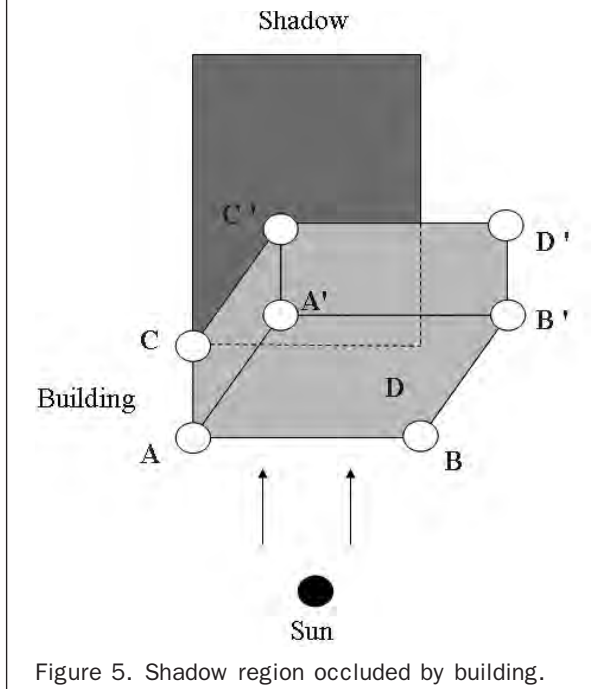

Figure 5. Shadow region occluded by building.

respectively. The building polygon was generated by points A′, B′, C′, D′, A, B, C, and D.

$$x = x_o - f \cdot \frac{r_{11}(X - X_s) + r_{12}(Y - Y_s) + r_{13}(Z - Z_s)}{r_{31}(X - X_s) + r_{32}(Y - Y_s) + r_{33}(Z - Z_s)} \quad (1)$$

$$y = y_o - f \cdot \frac{r_{21}(X - X_s) + r_{22}(Y - Y_s) + r_{23}(Z - Z_s)}{r_{31}(X - X_s) + r_{32}(Y - Y_s) + r_{33}(Z - Z_s)} \quad (2)$$

where, x_o and y_o are image coordinates of the principal point, f is the camera focal length; X_s, Y_s and Z_s are ground coordinates of perspective center, and r_{11}, r_{12}, . . . r_{33} are the elements of the rotation matrix.

Assessment of Shadow Detection Result

To assess the accuracy of the shadow detection algorithm, shadows in the corresponding aerial color image were compared to the output. For this purpose, a volunteer was recruited to manually delineate the shadowed regions in the aerial image based on the patterns of the reduced grey values. This practitioner was experienced in interpreting aerial images, apart from being given instructions for this work. A comparison of the regions marked by the human volunteer to those delineated by the proposed shadow detection algorithm showed that the overall accuracy of was 95.16 percent. Table 1 illustrates the results of the shadow detection. The number in Table 1 represents the pixels that were extracted using the proposed method and manual extraction. The errors (whether detected or not) that occurred upon using the proposed algorithms were mainly caused by the error of building height from lidar data. These errors are described by the following Equation, which is represented by geometry in Figure 3.

$$s = \frac{h}{\tan \alpha} \quad (3)$$

where, h means building height, α is the solar elevation angle, and s is the length of shadow.

As generally known, the vertical error of lidar data was ±15 cm (Cowen *et al.*, 2000) and solar elevation angle was 29.793°. Therefore, the influence caused by elevation error was approximately 0.28 m. Because the ground resolution was 0.25 m/pixel, the wrong or undetected pixel of shadow region was ±1 to 2 pixels. Furthermore, it was assumed that the mapping error of buildings from the digital map, DEM error, and geometric correction error of the aerial image could influence shadowing in the detection.

Segmentation of Shadowed Regions

The segmentation of shadows is very important because the results of segmentation have a direct effect on the correction of shadow-effects. Shadow regions contain many different surface cover types. Each cover type has a different spectral reflectance. The degree of influence interfered by shadow also varies for each surface type. Therefore, segmentation task is necessary. Polidorio *et al.* (2003) suggested a technique to segment shaded areas in aerial color images. This method is based on the physical phenomenon of atmospheric dispersion of Sun light, most popularly known as the Rayleigh scattering effect. Because the result showed that shadow regions were not clearly segmented, this method was not relevant. In this study, digital maps were utilized for segmentation. By overlapping the extracted shadow region and polygons representing each surface type from the digital map, the segmentation task was implemented.

TABLE 1. ERROR MATRIX RESULTING FROM SHADOW DETECTION

Category		(Units: Number of Pixels)		
		Reference Data		
		Shadow	Non-Shadow	Total
Modeling Data	Shadow	571,963	15,144	587,107
	Non-Shadow	13,925	–	13,925
	Total	585,888	15,144	–

Algorithms for Shadow Effect Correction

Stockham (1972) recognized that an image mainly is determined by two factors: the amount of solar radiation impinging on the land surface and the amount of image point to reflect light. These are called illumination and reflectance factors. The image could be modeled as a product of two components, $I_{i,j} = r_{i,j} \times L_{i,j}$. The parameter, $L_{i,j}$, represents the illumination source, while $r_{i,j}$ is the reflectance function of the image. The model of the image hindered by a shadow could be expressed as $I'_{i,j} = \alpha_{i,j} \times r_{i,j} \times L_{i,j}$. To generate a shadow-free image, the attenuation factor of the shadow, $\alpha_{i,j}$, must be calculated and removed.

For this study, the equation, $I'_{i,j} = \alpha_{i,j} r_{i,j} L_{i,j}$, was modified as follows:

$$\frac{I'_{i,j}}{\alpha_{i,j}} = r_{i,j} L_{i,j} \quad (4)$$

$$\frac{I'_{i,j}}{\alpha_{i,j}} = I'_{i,j} - I'_{i,j}\left(1 - \frac{1}{\alpha_{i,j}}\right) \quad (5)$$

$$I'_{i,j} - I'_{i,j}\left(1 - \frac{1}{\alpha_{i,j}}\right) = r_{i,j} L_{i,j} \quad (6)$$

$$I'_{i,j} + k_{i,j} = r_{i,j} L_{i,j} \quad (7)$$

$$I'_{i,j} + k_{i,j} = I_{i,j} \quad (8)$$

where i, j is the row and column number of the image, and $k_{i,j}$ is $-I'_{i,j}\left(1 - \frac{1}{\alpha_{i,j}}\right)$.

Equation 8 means that the original pixel not hindered by shadow could be reconstructed by correcting the factor, $k_{i,j}$, to the pixel interfered by shadow. In this study, the correction factor was defined as $k_{i,j}$. Finally, if the correction factors for each segmented shadow region were calculated, then the correction of the shadow effect would be possible. The correction factor could be calculated by obtaining the difference between the average of the shadow region and the average of the same surface type region, which is shadow-free.

Before applying Equation 8 to the correction of the shadow effect, three basic assumptions to accomplish shadow treatment in aerial images were considered. These were:

- Complete information loss of region hindered by shadow does not occur.
- The influence of cast shadow caused by each object is uniform.
- The DN value of similar surface cover characteristic is uniform.

The first assumption considers that the DN values of the shadowed area must not be zero. If the DN values were zero, the recovery of original information would be impossible. In reality, the range of image values of shadow regions is not

zero, but very low in satellite and aerial images. The second assumption means that the influence of cast shadow caused by blocking of the building must be uniform. Strictly speaking, the influence of shadows near the building is more intensive than that of shadows that are located relatively further from the building; however, the difference is very small. Based on this assumption, only one correction factor could be applicable to radiometric correction for segmented shadow areas. The third assumption explains that the standard deviation of DN values representing one segmented shadow region must be almost zero. If so, the accurate correction of the shadow effect could be possible. In reality, one segmented feature of shadow regions in aerial image shows the slight difference of DN values.

Equation 9 was applied for this study:

$$k_{i,j} = I_{i,j} - I'_{i,j} \tag{9}$$

where $k_{i,j}$ is the correction factor, $I'_{i,j}$ is the mean value of the shadowed target area, and $I_{i,j}$ is the mean value of the non-shadowed reference area.

In Equation 9, "shadowed target area" means the shadowed region to correct while "non-shadow reference area" represents the corresponding non-shadowed region.

Results of Shadow-Effect Correction

In Plate 2a, the corrected image was created using the proposed algorithm. In comparison with the original image, the result showed enhanced interpretability of the aerial color image. The radiometric correction of the asphalt road was very successful. The regions with diverse and complex ground features showed relatively low correction effects. For example, a parking lot made of paved asphalt included randomly distributed cars, but it was not a unique single polygon on the digital map; erroneous correction of the shadow effect occurred accordingly. From the viewpoint of the interpretation of urban facilities, its influence could be ignored. Figure 6 gives the average value of main surface cover types before and after the application of shadow effect correction. The range of the average value is 0 to 255. The test was implemented using the conventional histogram matching technique shown in Plate 2b. A detailed investigation of the results revealed some differences: specifically, the box area in Plate 2b is erroneously corrected. The box area represents the asphalt road, and the blue region, soil. Because the segmented shadows have different degrees of intensity, erroneous correction might be implemented in the case of removing the shadow effects using radiometric enhancement, especially in color images.

Potential Application to Road Extraction

The correction of shadow effects is a very critical procedure in image visualization and feature extraction. To show the potential applications of the proposed method in road extraction, it was implemented a second time using an aerial color image and lidar data without using digital maps in a simplified way without segmentation. First, the lidar point data were converted to raster data using kriging interpolation for DSM generation. Figure 7 shows the results of shadow detection using DSM generated by lidar. In Plate 3, the shadow region including the asphalt road is corrected by proposed shadow-effect correction method. In this case, the correction factor related to the asphalt road was used because the experiment's intent was not to visualize image but to extract the road.

In Figure 8, road extraction was implemented using the region growing method before and after the correction of the shadow effect. In Figure 8a, after the shadow-effect correction, the roads are detected including shadow regions. However, in Figure 8b, shadow regions assumed as roads are not detected. The results of the experiments are used as intermediate data for accurate road extraction.

Conclusions

In this paper, an experiment was conducted to show the effectiveness of the proposed algorithm for correcting shadow effects to enhance the interpretability of aerial color images using multi-source data sets. To delineate the shadowed regions in the image, shadow region detection was implemented using lidar data and digital maps. For

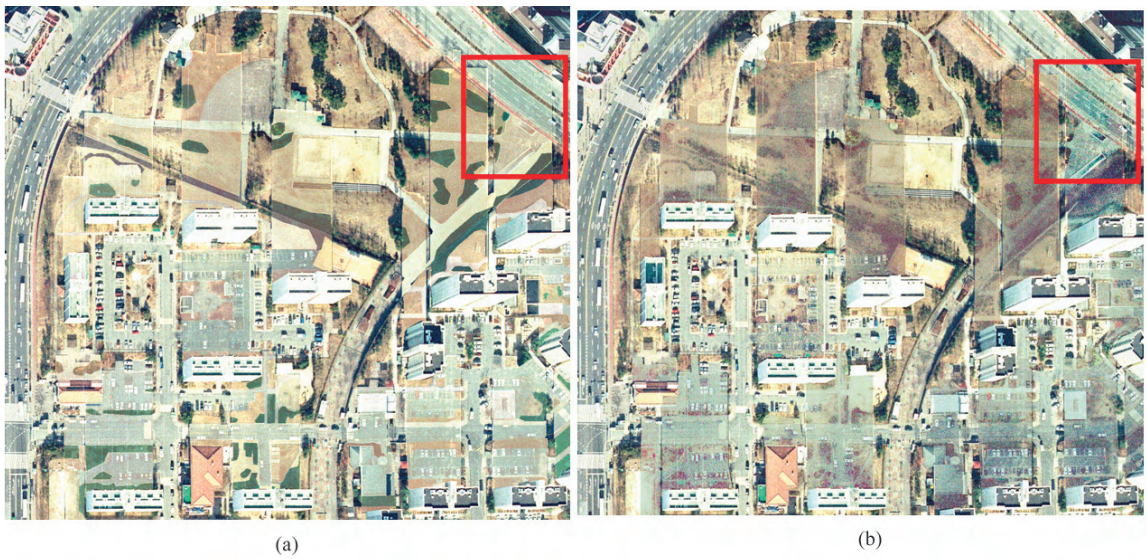

(a) (b)

Plate 2. Shadow-free image: (a) is ruled by proposed method, and (b) is ruled by radiometric enhancement.

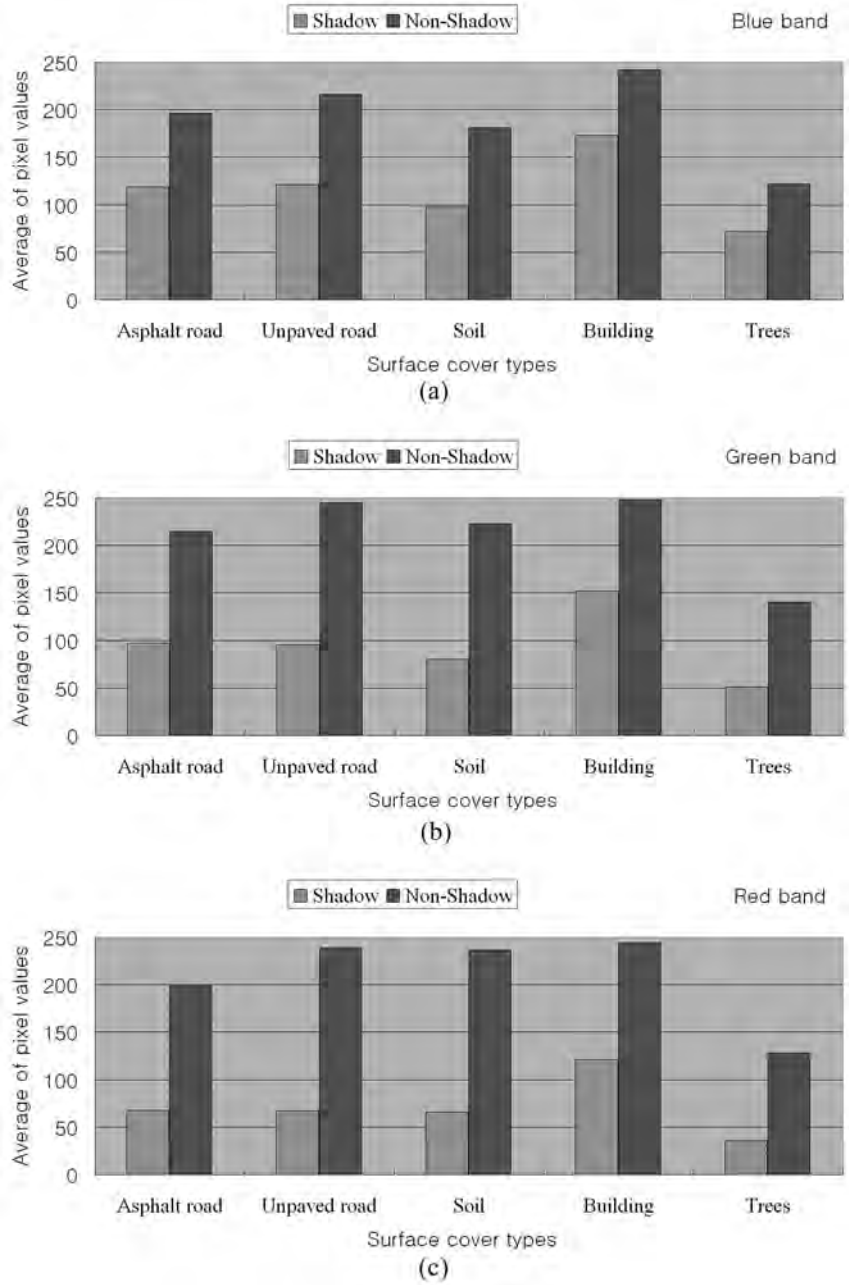

Figure 6. Average of pixel values in shadow and non-shadow region.: (a) blue band, (b) green band, and (c) red band.

more accurate shadow detection, 3D city modeling is required. Rigorous 3D city modeling using lidar data can depict the city's appearance, including complex shaped buildings. Rigorous 3D city modeling is not yet perfect, and is still very complex. Recently used techniques for removing shadows, such as radiometric enhancement in high-resolution images, are based on histogram treatment. In the test described in this paper, these methods showed somewhat improved interpretability. The results depended heavily, however, on the image content. The algorithms proposed in this paper are comparatively simple, as they use merely the relationship between the same land surface types (i.e., the same surface types in the shadowed and shadow-free areas) and are less image-dependent, because the shadows can be segmented according to the land surface type and the segmented shadows can be directly corrected by comparing them with the corresponding same non-shadow region.

References

Adler-Golden, S.M., M.W. Matthew, G.P. Anderson, G.W. Felde, and J.A. Gardner, 2002. An algorithm for de-shadowing spectral imagery, *Proceedings of the 11th JPL Airborne Earth Science Workshop*, 05–08 March, Pasadena, California, JPL Publication, pp. 3–4

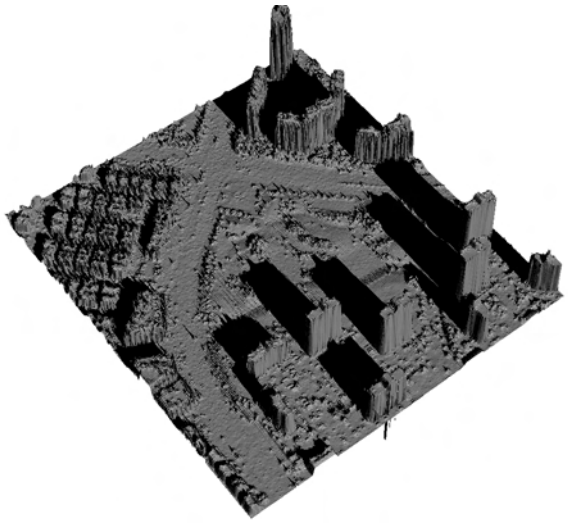

Figure 7. Extraction of shadow regions using only lidar.

Boardman, J.W., 1993. Automated spectral unmixing of AVIRIS data using convex geometry concepts, *Summaries of Fourth JPL Airborne Geoscience Workshop*, 25–29 October, Washington, D.C., Pasadena, California, JPL publication, pp. 11–14.

Civco, D.L., 1989. Topographic normalization of Landsat Thematic Mapper Digital Imagery, *Photogrammetric Engineering & Remote Sensing*, 55(9):1303–1309.

Colby, J.D., 1991. Topographic normalization in rugged terrain, *Photogrammetric Engineering & Remote Sensing*, 57(5):531–537.

Cowen, D.J., J.R. Jensen, C. Hendrix, M.E. Hodgson, and S.R. Schill, 2000. A GIS-assisted rail construction econometric model that incorporates LIDAR data, *Photogrammetric Engineering & Remote Sensing*, 66(11):1323–1328.

Dare, P.M., 2005. Shadow analysis in high-resolution satellite imagery of urban areas, *Photogrammetric Engineering & Remote Sensing*, 71(2):165–177.

Plate 3. Corrected image focused on asphalt road

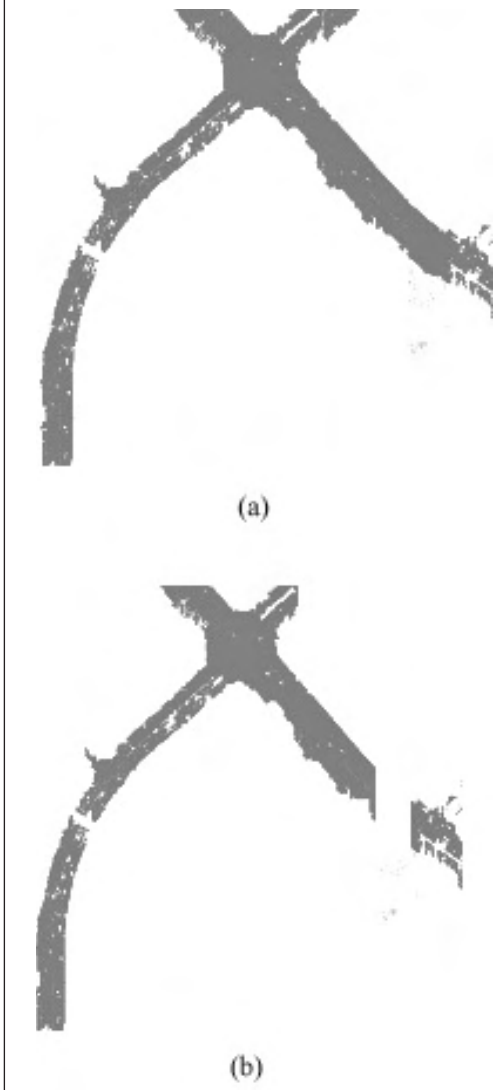

Figure 8. The results of road extraction using region growing method: (a) Extraction from the shadow-corrected aerial image, and (b) Extraction from the original aerial image.

Giles, P., 2001. Remote sensing and cast shadows in mountainous terrain, *Photogrammetric Engineering & Remote Sensing*, 67(7):833–839.

Hall-Konyves, K., 1987. The topographic effect on Landsat data in gently undulating terrain in southern Sweden, *International Journal of Remote Sensing*, 8(2):157–168.

Itten, K.I., and P. Meyer, 1993. Geometric and radiometric correction of TM data of mountainous forested areas, *IEEE Transactions on Geoscience and Remote Sensing*, 31(4):729–748.

Kawata, Y., S. Ueno, and T. Kusaka, 1998. Radiometric correction for atmospheric and topographic effects on Landsat MSS images, *International Journal of Remote Sensing*, 9(4):729–748.

Lui, J.G., and J.M. Moore, 1993. Cloud shadow suppression technique for enhancement of airborne thematic mapper imagery, *Photogrammetric Engineering & Remote Sensing*, 59(8):1287–1291.

Polidorio, A.M, F.C. Flores, N.N. Imai, A.M.G. Tommaselli, and C. Fransco, 2003. Automatic shadow segmentation in aerial color images, *Proceeding of the XVI Brazilian Symposium on Computer Graphics and Image Processing*, pp. 270–277.

Pouch, G.W., and D.J. Campagna, 1990. Hyperspherical direction cosine transformation for separation of spectral and illumination information in digital scanner data, *Photogrammetric Engineering & Remote Sensing*, 56(4):475–479.

Rau, J.Y., N.Y., Chen, and L.C. Chen, 2002. True orthophoto generation of built-up areas using multi-view images, *Photogrammetric Engineering & Remote Sensing*, 68(6):581–588.

Richter, R., 1998. Correction of satellite imagery over mountainous terrain, *Applied Optics*, 37(18):4004–4015.

Shu J.S.-P., and H. Freeman, 1990. Cloud shadow removal from aerial photographs, *Pattern Recognition*, 23(6):647–656.

Simpson, J.J., and J.R. Stitt, 1998. A procedure for the detection and removal of cloud shadow from AVHRR data overland, *IEEE Transactions on Geoscience and Remote Sensing*, 36(3):880–897.

Stockham, J.T.G., 1972. Image processing in the context of a visual model, *Proceedings of the IEEE*, 60:828–842.

Wang, B., A. Ono, K. Muramatsu, and N. Fujiwara, 1999 Automated detection and removal of clouds and their shadows from Landsat TM images, *IEICE Transactions on Information and Systems*, E82D(2):453–460.

(Received 08 November 2005; accepted 22 March 2006; revised 13 September 2006)